The 56th International October Conference on Mining and Metallurgy
22-25 October 2025, Bor Lake, Bor, Serbia
www.ioc.tfbor.bg.ac.rs

DOI: 10.5937/IOC25364B *Original scientific paper*

MICROSTRUCTURAL ANALYSIS AND THERMAL PROPERTIES OF Ag-Sn ALLOYS

Kristina Božinović[1a], Dragan Manasijević[1b], Ljubiša Balanović[1c], Milan Gorgievski[1d], Uroš Stamenković[1e], Miljan Marković[1f]

[1] Technical Faculty Bor, University of Belgrade, V.J. 12, 19210 Bor, Serbia
[1a] kbozinovic@tfbor.bg.ac.rs, 0000-0002-9834-448X
[1b] dmanasijevic@tfbor.bg.ac.rs, 0000-0002-7828-8994
[1c] ljbalanovic@tfbor.bg.ac.rs, 0000-0002-3551-6731
[1d] mgorgievski@tfbor.bg.ac.rs, 0000-0002-9899-719X
[1e] ustamenkovic@tfbor.bg.ac.rs, 0000-0002-7579-2159
[1f] mmarkovic@tfbor.bg.ac.rs, 0000-0002-4734-1481

Abstract
The Ag–Sn system represents one of the most significant binary alloy systems in the development of lead-free solder materials and high-performance electronic interconnections. In this study, thermal properties, microstructural evolution, and thermodynamic behavior of the Ag–Sn system were investigated. Alloys were synthesized from high-purity Ag and Sn and characterized using differential scanning calorimetry (DSC), flash method for the analysis of thermal properties (DXF) and scanning electron microscopy with energy dispersive spectroscopy (SEM-EDS), enabling precise determination of phase transitions and microstructural features across the composition range. The obtained results were compared with available thermodynamic assessments and phase diagram data, highlighting both agreements and discrepancies in reported invariant reactions. The findings contribute to a deeper understanding of the solidification paths and stability of phases in Ag–Sn alloys, which is of particular importance for optimizing solder joint reliability in microelectronic applications.

Keywords*: Ag–Sn alloys, microstructure, thermal conductivity, electrical conductivity, microhardness*

1. INTRODUCTION

For more than two decades, since the RoHS directive was introduced [1], the scientific community has been in pursue of the suitable replacement for Sn-Pb soldering alloy [2]. The last couple of years the research was aimed on the third-generation Pb-free solders, focusing on alloys with high Ag content among the other ones [2-4]. The third-generation Pb-free solders emerged when a need for high reliability solders arose with the development of vehicle electronics. Dynamic, "under the hood" conditions limited the usage of the globally used near-eutectic SAC alloys, because of their poor resistance to mechanical shock [2, 4-6].

The Ag–Sn system represents one of the most significant binary alloy systems in the development of lead-free solder materials and high-performance electronic interconnections [1, 2]. As a part of a ternary Sn-Ag-Cu system (SAC), this system has been of interest and therefore investigated numerous times [1-6]. The researches were mainly focusing on the eutectic Sn-3.5 mass%Ag alloy and there are only few investigations considering the influence of Ag content on the properties of alloys [3, 7]. Even so, the content of silver was always relatively low with most of the interest on low-Ag alloys, taking the economic variable into account. The low-Ag composition, which corresponds to near-eutectic SAC alloys, has already been investigated, and it is well established that these alloys exhibit poor thermal fatigue resistance, therefore not suitable for "under the hood" conditions of severe thermal cycling [8, 10]. Therefore, the focus of this paper will be the influence of Ag content on alloy properties but from a different point of the Ag-Sn phase diagram (Ag based).

Special attention was given to thermo-physical properties of the regarded system, most importantly thermal conductivity, thermal diffusivity and specific heat capacity as contribution to a more complete knowledge of the thermal transfer behavior of these alloys.

2. EXPERIMENTAL

The metals used for the preparation of selected samples (Table 1) were silver and tin of > 99.9% purity (Alfa Aesar). Investigated alloys were prepared by melting weighted masses of pure metals in a chamber furnace under inert argon atmosphere at maximum temperature of 1100 °C. The total masses of the prepared samples were about 2 g. After melting and stirring, the molten alloys were allowed to solidify into graphite crucibles. Prepared alloy ingots were re-melted at least 3 times to assure homogeneous compositions. The obtained samples were cut into two parts. Smaller part of the sample was used for DSC analysis, and the remaining part was pressed on a hydraulic press to obtain samples of the same dimensions, a tablet shape of 12.7 mm in diameter. The sample with the highest Ag content was pressed with the force of 10 kN. After pressing, annealing was done in order to perform recovery and recrystallization, remove internal stresses and micro segregations. The annealing was carried out at 500 °C, in a closed chamber furnace, in a protected atmosphere, for 24^{h}. For the other samples, brittleness caused by deformation hardening in combination with the formed intermetallic compounds, was noticed, increasing with the increase of Sn content. For other samples, the cycling combination of pressing and annealing was done in order to obtain the dimension of the samples required for further testing.

The annealed samples were then used for investigation of thermal conductivity and diffusivity, electrical conductivity and structural investigation. Microstructural observations were carried out using a combined application of optical microscopy and SEM accompanying with EDS energy-dispersive X-ray spectrometry (EDS) was used for composition determination and identification of coexisting phases. Light optical microscopy was performed by using a Carl Zeiss Jena Epityp 2 microscope. The samples were prepared through three steps including grinding, polishing and structure development (etching solution of $K_2Cr_2O_7$ in H_2SO_4). SEM–EDS analysis was performed on a TESCAN VEGA3 scanning electron microscope operated at 20 kV. The EDS (Oxford Instruments X-act) was employed for measurements of overall compositions and compositions of individual phases. The TGA–DSC/DTA simultaneous thermal analyzer (TA Instruments SDT Q600) was used for the investigation of melting and phase transformation temperatures. The instrument was calibrated by measuring the melting temperatures and the heat of melting of standard materials (pure metals: Ag and Sn). The measurements were performed in an argon atmosphere. The masses of the samples were about 10–20 mg, and a heating rate was $10°Cmin^{-1}$. Thermal diffusivity was measured by using Discovery Xenon Flash (DXF-500) instrument over a range of temperatures from 25 to 400 °C. Thermal conductivity of the investigated samples was determined using the following relation:

$$\lambda = \alpha \cdot \rho \cdot C_p \tag{1}$$

where λ is thermal conductivity ($Wm^{-1}K^{-1}$), α is thermal diffusivity (m^2s^{-1}), ρ is density (kgm^{-3}) and Cp is the calculated specific heat capacity ($Jkg^{-1}K^{-1}$). The densities of the investigated alloys at room temperature were determined using the indirect Archimedean method, following the procedure outlined in previous research [15]. The specific heat capacities were evaluated through the CALPHAD approach [16], employing optimized thermodynamic parameters from the COST 531 lead-free solder thermodynamic database [17]. Electrical conductivity was measured using the Foerster SIGMATEST 2.069 instrument. Based on the measured value of thermal and electrical conductivities at the room temperature and Wiedemann–Franz law (2), electronic and phonon contributions to the thermal conductivity of studied alloys were calculated.

$$\frac{\lambda}{\sigma} = \mathrm{L} \cdot \mathrm{T} \quad (2)$$

The microhardness of the samples was evaluated by the Vickers method in accordance with the ASTM E384 standard [18], using a PMT-3 Vickers microhardness tester.

3. RESULTS AND DISCUSSION

Identified individual phases based on the results of SEM/EDS analysis for all alloys are given in Table 1 along with the composition of the investigated alloys.

Figure 1a, c and e illustrate microstructures of the samples, while the 1b, d and f showcase the detailed microstructures of the same alloys on high-magnification SEM micrographs. The calculated equilibrium (Lever Rule) and non-equilibrium (Scheil model) solidification paths for the studied alloys were used as an aid in the analysis of as-solidified microstructures of the Ag - Sn alloys. The equilibrium and non-equilibrium solidification paths were calculated using thermodynamic parameters from [17].

Table 1.Molar composition of investigated alloys in Ag-Sn system, overall composition and identified individual phases based on the results of SEM/EDS analysis

Sample label	Nominal composition		Composition		Identified phases
	Ag/at%	Sn/at%	Ag/at%	Sn/at%	
A1	95	5	95.11	4.89	(Ag)
A2	89	11	89.34	10.66	(Ag) + ζ
A3	85	15	85.40	14.60	ζ

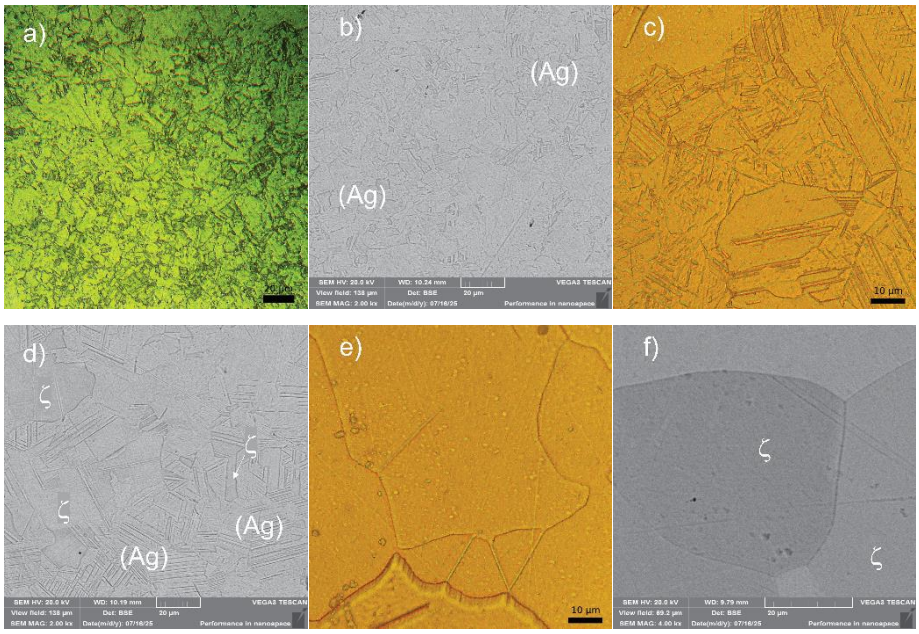

Figure 1. Optical and detailed micrographs of the samples: a), b) A1; c), d) A2 and e), f) A3

According to the results of thermodynamic calculations, equilibrium solidification (Figure 2) in all three cases begins with the precipitation of primary crystals of the (Ag) phase. For the sample A1, it is followed by solidification at around 720 °C in the same monophase area, which is confirmed by the results of the EDS (Table 1) and DSC (Table 2) analysis. The sample A2 follows the same path, however, ζ phase detected does not appear in the results of thermodynamic

calculations. Additionally, using thermodynamic parameters from [17], phase fraction diagram was calculated (Figure 2c). What must be taken into account here is the annealing at 500 °C. Therefore, the following thermodynamic calculations were observed at 500 °C and the experimental results were in a good agreement. According to the phase fraction diagram for alloy A2, bellow solidus temperature, (Ag) is stable until slightly below 650 °C. Bellow that point, due to the solid state reactions, stable phases are (Ag) and ζ, which were confirmed in the experimental process. The sample A3 also follows the path of equilibrium solidification, followed by the invariant reaction at 719.3 °C whereby the primarily formed crystals of the (Ag) phase react with the liquid: Liq + (Ag) → ζ. The remaining melt solidifies at around 683 °C, in ζ monophase area, which is also confirmed by the results of the EDS and DSC analysis.

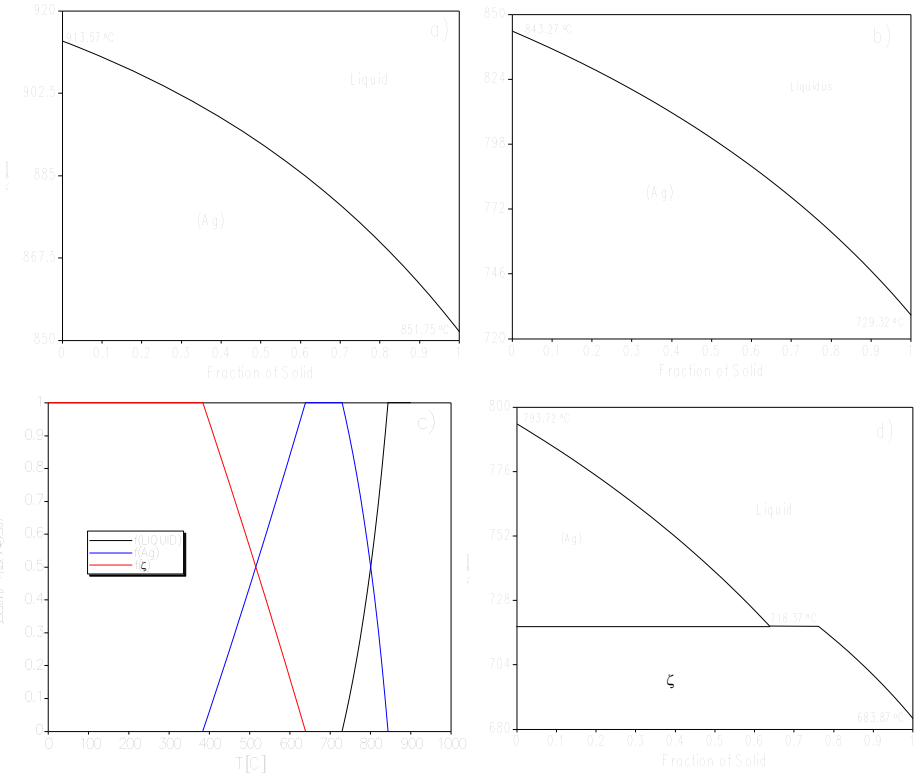

Figure 2. Equilibrium (Lever Rule) solidification paths simulation of samples: a) A1, b) A2, c) A2 – phase fraction diagram, d) A3

The solidus temperature was determined from the extrapolated onset of the first heating peak, while the liquidus temperature corresponded to the peak temperature of the final thermal event. The melting behavior of all alloys is summarized in Table 2, with representative DSC heating curve for sample A2 shown in Fig. 3. For the sample A3, due to the close proximity of the solidification and peritectic reactions, only one peak is distinguished in the thermogram at 727 °C.

Table 2. Phase transitions temperatures for examined alloy compositions obtained by the DSC analysis and comparison with thermodynamic calculation

Sample label	Experimental phase transition temperatures /°C		Calculated phase transition temperatures (equilibrium) /°C		
	solidus	liquidus	solidus	peritectic reaction [19]	liquidus
A1	872.06	921.11	851.75	/	913.57
A2	727.56	855.78	729.32	724	843.27
A3	723.54	822.72	683.87	724	793.72

Experimentally determined densities of investigated alloys, used in the further calculation of thermal properties, are presented graphically as a dependence of the composition in Figure 4.

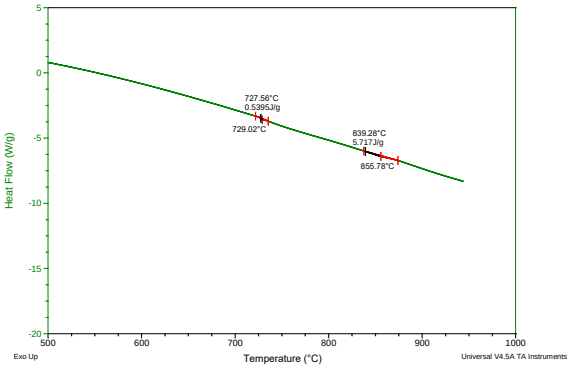

Figure 3 - DSC heating curve for alloy A2

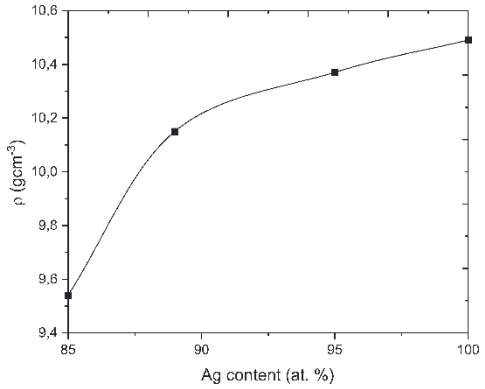

Figure 4 - Experimentally determined densities of investigated alloys

Calculated and experimentally obtained values of thermal diffusivity, specific heat capacity and thermal conductivity for the samples A1 and A2, investigated in the temperature range from 25 to 400 °C, are given in Table 3. In spite of all efforts, sample A3 did not reach the desired dimension due to brittleness, therefore couldn't be used for thermal properties investigations.

Both Ag–Sn alloys show a slight increase in specific heat capacity with temperature, with little difference between A1 and A2, indicating that Sn addition has minimal effect on this property. In contrast, thermal diffusivity and conductivity are strongly composition dependent. The sample A1 exhibits higher values compared to A2 across the 25–400 °C temperature range, however, compared to pure silver, which is considered to be the best heat conductor of all metals, both alloys show markedly reduced values. The higher Sn content diminishes the electronic contribution to heat transfer and enhances scattering effects, which together limit thermal transport. Consequently, increasing the Sn fraction leads to reduced thermal diffusivity and conductivity, while the heat capacity remains almost unaffected. This makes the Ag-rich alloys more advantageous for applications where efficient thermal management is critical.

Table 3. Specific heat capacity, thermal diffusivity, and thermal conductivity of the investigated Ag -Sn alloys in the temperature range 25–400 °C.

Sample label	Temperature /°C	Specific heat capacity /$Jg^{-1}K^{-1}$	Thermal diffusivity /mm^2s^{-1}	Thermal conductivity /$Wm^{-1}K^{-1}$
A1	25	0.235	12.8	31.18
	100	0.238	13.9	34.39
	200	0.243	15.5	39.07
	300	0.248	17.0	43.65
	400	0.253	18.7	49.12
A2	25	0.234	7.6	18.24
	100	0.239	8.7	21.09
	200	0.244	9.9	24.62
	300	0.248	10.9	27.41
	400	0.252	11.5	29.48

The results of the electrical conductivity measurements are given in Table 4 along with the results of microhardness testing. The microhardness measurements show a clear growth with increase of Sn content. This strengthening effect is attributed to the higher fraction of intermetallic phases (ζ) that form with increasing Sn concentration. These phase is inherently harder and less ductile than the Ag matrix, thereby increasing resistance to localized plastic deformation. In addition, the repeated pressing–annealing cycles applied to A2 and A3 during preparation may have further contributed to hardening through deformation-induced defects and microstructural refinement.

Table 4. Electrical conductivity measurements. calculations based on Wiedemann-Franz law and the results of microhardness testing

Alloy	σ /MSm^{-1}	λe /WmK^{-1}	λe/%	λph /WmK^{-1}	λph /%	$HV_{0.1}$
A1	4.8 ± 0.15	34.90	89	11	3.72	78.62
A2	4.7 ± 0.11	34.17	53	47	15.93	104.42
A3	4.5 ± 0.08	/	/	/	/	126.65

The electrical conductivity measurements show only a slight decrease with increasing Sn content. Calculations based on the Wiedemann–Franz law indicate that in alloy A1, thermal conductivity is predominantly governed by the electronic contribution, with a much smaller share from phonons. In contrast, alloy A2 shows a reduced electronic contribution and a significantly larger phonon contribution, highlighting the strong effect of higher Sn content on heat transport mechanisms. This shift reflects enhanced scattering and reduced electron mobility in A2, which lowers the dominance of electronic thermal conduction and increases the relative role of phonons. Thus, while overall electrical conductivity decreases only moderately, the balance between electronic and phonon contributions to thermal transport changes considerably with composition.

4. CONCLUSION

The results show that alloy composition and preparation route both play a decisive role in determining the properties of Ag–Sn alloys. While A1 (Ag–5Sn) was sufficiently ductile to be pressed and annealed once, A2 (Ag–11Sn) and A3 (Ag–15Sn) exhibited brittleness due to deformation hardening and intermetallic formation, requiring repeated pressing–annealing cycles to achieve workable samples. Microstructural analysis confirmed that solidification is dominated by (Ag) primary phase formation, with increasing Sn content leading to the appearance of ζ intermetallic phase. Thermal characterization revealed that specific heat capacity is only slightly affected by Sn, whereas thermal diffusivity and conductivity decrease sharply with the addition of tin, a consequence of reduced electronic heat transport and stronger scattering. Electrical conductivity dropped only moderately, but the Wiedemann–Franz analysis highlighted a transition from electron-dominated to more phonon-influenced heat conduction. Microhardness measurements confirmed strengthening due to the higher Sn content, correlating with intermetallic formation and processing-induced hardening. Overall, Ag-rich alloys such as Ag–5Sn retain slightly higher thermal conductivity and good mechanical stability, making them preferable for applications where reliable thermal management is essential, while higher Sn contents increase hardness at the expense of thermal efficiency and processability.

ACKNOWLEDGEMENTS

The research presented in this paper was done with the financial support of the Ministry of Science. Technological Development and Innovation of the Republic of Serbia. within the funding of the scientific research work at the University of Belgrade - Technical Faculty in Bor. according to the contract with registration number 451-03-137/2025-03/200131.

REFERENCES

[1] Restriction of Hazardous Substances in Electrical and Electronic Equipment (RoHS). https:// envir onment. ec. europa. eu/ topics/waste- and- recyc ling/ rohs- direc tive_ en. Accessed 01 Aug 2025.
[2] W.N.C. Weng. Evolution of Pb-free solders. In: Mohamad. AA editor. Recent Progress in Soldering Materials. 1st ed.. 2017. 91–108.
[3] K. Božinović. D. Manasijević. L. Balanović. I. Marković. M. Gorgievski. U. Stamenković. M. Marković. JTAC. (2025) pp.1-18.
[4] E. Dalton. G. Ren. J. Punch. M.N. Collins. Mater. Des.. 154 (2018) 184-191.
[5] R. Coyle. M. Reid. C. Ryan. R. Popowich. P. Read. D. Fleming. et al.. "The influence of the Pb-free solder alloy composition and processing parameters on thermal fatigue performance of a ceramic chip

resistor." in Electronic Components and Technology Conference. 2009. ECTC 2009. 59th. 2009. pp 423-430.
[6] D.A. Shnawah. M.F.M. Sabri. I.A. Badruddin. Microelectronics Reliab.. 52 (2012) 90-99.
[7] D. Manasijević. L. Balanović. I. Marković. M. Gorgievski. U. Stamenković. A. Đorđević. D. Minić. V. Ćosović. Solid State Sci.. 119 (2021) 106685.
[8] R. Novakovic. S. Delsante. J. Lee. G. Borzone. J. Mater. Sci.: Mater. Electron.. 29(20) (2018) 17108-17121.
[9] K. Suganuma. S.H. Huh. K. Kim. H. Nakase. Y. Nakamura. Mater. Trans.. 42 (2) (2001) 286-291.
[10] E. Çadırlı. M. Şahin. R. Kayalı. M. Arı. S. Durmuş. 2011. J. Mater. Sci.: Mater. Electron.. 22 (11) (2011) 1709-1714.
[11] S. Choi. T.R. Bieler. K.N. Subramanian. J.P. Lucas. SMT. 13 (2) (2001) 26-29.
[12] F. Meydaneri. B. Saatçi. M. Ozdemir. Kovove Mater.. 51 (2013) 173-181.
[13] P. Fima. Appl. Surf. Sci.. 257 (8) (2011) 3265-3268.
[14] M. Reid. J. Punch. M. Collins. C. Ryan. SMT. 20 (2008) 3-8.
[15] D. Manasijević. L. Balanović. I. Marković. M. Gorgievski. U. Stamenković. K. Božinović Thermochim. Acta. (2021).
[16] H.L. Lukas. S.G. Fries. B. Sundman Computational Thermodynamics: the Calphad Method. Cambridge: Cambridge University Press; 2007.
[17] A. Kroupa. A. Dinsdale. A. Watson. J. Vrestal. J. Vízdal. A. Zemanova JOM (2007).
[18] ASTM:E384-10. „Standard test method for Knoop and Vickers hardness of materials. ASTM international. West Conshohocken. USA.“ 2010.
[19] I. Karakaya. W. T. Thompson. Bull. Alloy Phase Diagrams. 8 (1987). 340-347.